Journal of Muscle Research and Cell Motility **17**, 221–233 (1996)

Mechanics of feline soleus: II Design and validation of a mathematical model

IAN E. BROWN, STEPHEN H. SCOTT[‡], and GERALD E. LOEB*

The MRC Group in Sensory-Motor Neuroscience, Department of Physiology, Queen's University, Kingston, Ontario, Canada K7L 3N6

Received 3 July 1995; revised 18 October 1995; accepted 23 October 1995

Summary

We have developed a mathematical model to describe force production in cat soleus during steady-state activation over a range of fascicle lengths and velocities. The model was based primarily upon a three element design by Zajac but also considered the many different features present in other previously described models. We compared quantitatively the usefulness of these features and putative relationships to account for a set of force and length data from cat soleus whole-muscle described in a companion paper. Among the novel features that proved useful were the inclusion of a short-length passive force resisting compression, a new normalisation constant for connective-tissue lengths to replace the potentially troublesome slack length, and a new length dependent term for lengthening velocities in the force-velocity relationship. Each feature of this model was chosen to provide the most accurate description of the data possible without adding unneeded complexity. Previously described functions were compared with novel functions to determine the best description of the experimental data for each of the elements in the model.

Introduction

Mathematical models of muscle help us to understand and develop strategies for motor control, both for pure research and for clinical restoration of movement to paralysed limbs through functional electrical stimulation (FES) (see Chizeck, 1992). Open loop controllers for FES require a muscle model that can predict the activation needed to achieve a desired force output from muscle under various kinematic conditions. Very few models, however, have been able to describe accurately a muscle's response to activation even for the architecturally simple muscles. A common problem with most models is that they do not describe muscle behaviour adequately over their full physiological range of kinematics. Muscles are active over a range of lengths, and also over a range of shortening and lengthening velocities (Goslow *et al.*, 1973; Walmsley *et al.*, 1978; Loeb, 1985; Chanaud *et al.*, 1991). The very few models that have attempted to describe activated muscle under lengthening conditions (Mashima *et al.*, 1972; Hatze, 1977), were based on fragmentary data from a few diverse preparations including cat whole muscle, frog single fibres and frog fibre bundles (Joyce *et al.*, 1969; Mashima *et al.*, 1972; Sugi, 1972).

In a series of studies, a more complete set of experimental data was generated for cat soleus using modern instrumentation that permitted precise control of whole muscle length, velocity and activation plus accurate measurements of the lengths of fascicle, aponeurosis and tendon (hereafter collectively referred to as connective-tissues) during force generation (Scott & Loeb, 1995; Scott *et al.*, 1996). Data were collected under both passive and maximally (steady-state) active conditions. In the present study, the various components of the general model of muscle and connective-tissues suggested by Zajac (1989) were modelled with various mathematical functions. Some of these functions were suggested from previous studies, but others were newly generated to capture better the particular relationships observed in this new data-set. This paper compares the best-fits that could be obtained for these functions for both passive and steady-state, maximally active muscles.

*To whom correspondence should be addressed at: Bio-Medical Engineering Unit, Queen's University, Kingston, Ontario, Canada K7L 3N6.
‡Present Address: Dépt. de physiologie, Université de Montréal, Montréal, Québec, Canada H3C 3J7.

The model

The model elements chosen for this study are shown schematically in Fig. 1A. The model contains anatomically distinct elements. A series-elastic element (SE) represents the connective-tissues and a passive elastic element (PE) in parallel with an active contractile element (CE) represents the muscle fascicles. The properties of all three elements were examined in this study.

The SE was modelled as a non-linear spring (Zajac, 1989). The aponeurosis and tendon (also known as the internal and external tendons) were lumped together into one spring because their properties have been observed to be similar (Scott & Loeb, 1995).

The PE, as shown in Fig. 1B, has two spring-like components. When the slack is pulled out of the ideal, bendable, fixed-length linkage that connects spring PE1, it exerts a tensile force. At shorter fascicle lengths, the compression spring PE2 comes into play with a separate spring function that resists compression. The PE2 spring was included in the model in order to separate the active and passive components of muscle force output. There is substantial evidence that the active force in muscle is produced by the cumulative effect of multiple independent cross-bridge interactions (see Huxley, 1971). We assumed therefore that the shape of the active isometric force-length (FL) curve should be proportional to the total number of sites available for cross-bridge formation. By explicitly following this definition, the FL curve should look as shown in Fig. 2A (solid line), and not like the curve used by most authors (e.g. Gordon *et al.*, 1966) (dotted line). The discrepancy only occurs at short lengths on the ascending limb of the FL curve. The very steep

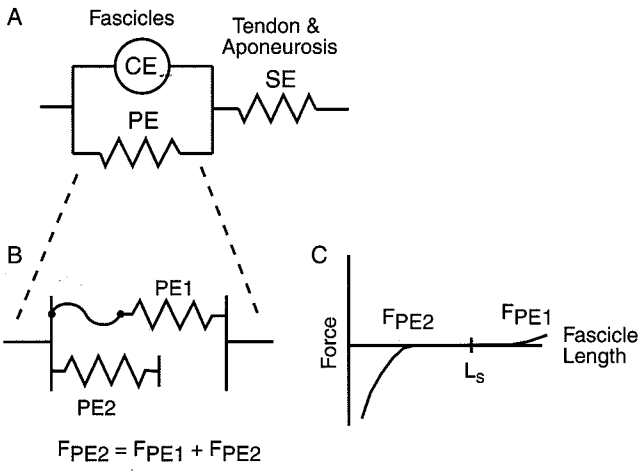

Fig. 1. (A) Schematic of muscle model elements (based on model from Zajac, 1989). (B, C) Parallel Elastic element. PE1 is well recognized non-linear spring resisting stretch, while PE2 is a non-linear spring resisting compression.

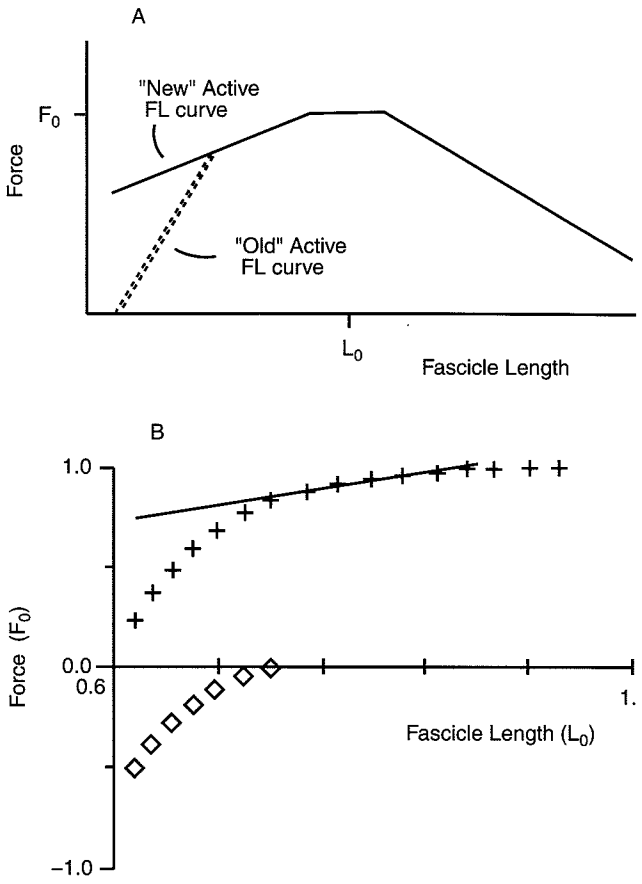

Fig. 2. (A) 'Old' active FL curve with steep portion of ascending limb and 'new' active FL curve with F_{PE2} removed. (B) Data from active FL trial (+). Solid line is an extrapolation of data from between 0.75 L_0 and 0.95 L_0. Difference between original data (+) and extrapolation is used as passive force (◇).

relationship measured on the ascending limb was explained by Gordon and colleagues to occur because the myosin filaments push against the Z-disks at short sarcomere lengths, thus producing a resistive force and reducing the total force. This pushing-resistive force produced by the myosin filaments on the Z-disk is presumably passive in nature because it is not produced directly by the cross-bridges. Two observations made by Allen and Moss (1987) in maximally activated skinned muscle fibres (Ca^{2+} activation) support this conclusion. The shape of Allen and Moss' recorded FL curve included a steep portion similar to that recorded by Gordon and colleagues indicating that the steep portion is not due to a decrease in activation (i.e. calcium release). Secondly, the ratio of stiffness-to-tension remained approximately constant as length decreased from L_0 (fascicle length at which maximal isometric force is observed) until ~ 0.75 L_0 at which point the ratio increased dramatically. Including this passive force as part of the active FL curve leads to errors under non-isometric conditions, because active

force is highly dependent upon cross-bridge velocity and activation while passive force is not.

The mathematical outline of the CE is summarized in Equation 1. The CE is assumed to be affected by three independent factors represented by the following functions: F_{ACT} (u(t), L?, V?), FL(L), and FV(L, V). F_{ACT} is a unitless measure between 0 (passive) and 1 (maximally active) of the muscle fascicles' activation. It depends on both the number of fibres activated and their transient state of activation as determined by the neuronal input (u(t)). Activation kinetics and hence F_{ACT} may depend also upon fascicle length (L) and/or fascicle velocity (V) (personal observation; Scott *et al.*, 1992). FL is the FL curve for the muscle fascicles (dependent upon fascicle length), and FV is the force-velocity curve for the muscle fascicles (dependent upon both fascicle length and velocity; Scott *et al.*, 1996). The inclusion of length as a variable in the FV curve is required to account for the observation that the active-lengthening and active-shortening regions of the force velocity curve cannot be scaled congruently for all lengths.

$$F_{CE} = F_{ACT}(u(t), L?, V?) * FL(L) * FV(L, V) \quad (1)$$

Normalisation constants for the force, length and velocity data were chosen as suggested by Zajac (1989) to facilitate scaling between different muscles. All fascicle data were normalized in terms of L_0 for length, and F_0 for force (the force produced during an isometric contraction at L_0). For consistency with the chosen length units, fascicle velocity was normalized to $L_0\,s^{-1}$. Although tradition would have velocity positive in the shortening direction, mathematically it should be defined as positive in the lengthening direction and was so defined for this model. Because F_{CE} has units of F_0, $F_{ACT} * FL * FV$ must also have units of F_0. F_{ACT} was defined to be unitless and FL was chosen to have units of F_0 thus the 'force' in the FV curve was defined as a unitless 'force index'. The connective-tissue lengths were also normalized to facilitate scaling between muscles but in a manner somewhat different from the approach used by Zajac (1989) and other previous studies (Hubbard & Chun, 1988; Lieber *et al.*, 1992). Connective-tissue (T) data were normalized in terms of F_0 for force and L_0^T for length (connective-tissue length at F_0) as opposed to the more commonly used L_s^T (connective-tissue slack length). The assumptions required to choose these normalization factors were that both the material properties of connective-tissue and the ratio of connective-tissue cross-sectional area (CSA) to muscle physiological cross-sectional area (PCSA) must be specimen independent (as per Zajac, 1989). The reasons for choosing L_0^T over L_s^T are discussed below.

Materials and methods

Data from *in vivo* experiments on cat soleus muscle (originally reported by Scott *et al.*, 1996) were used as the basis to develop and test model relationships. The data records consisted of connective-tissue lengths, fascicle lengths (from which fascicle velocity was calculated) and forces. Force was recorded by a strain gauge in series with the tendon and muscle puller while direct measurements were taken of the connective-tissue and fascicle lengths by the transit time of ultrasound pulses between piezoelectric crystals glued to the surface of the different structures. All data used in this study were obtained while the muscle was in a steady-state of activation at the end of a supra-maximal tetanic stimulus (400 ms train at 50 PPS, 4 × threshold applied to the muscle nerve), except as described below for determining the F_{SE} curve. Data used in this study included both passive and active trials for whole-muscle isometric trials (FL trials) over the physiological range of motion (ROM) and for whole-muscle isovelocity trials (FV trials) over a range of velocities and a range of lengths. In two of the experiments reported by Scott and colleagues (1996), the maximum active force recorded during the FL trials was from the FL trials' longest length, so that an L_0 was not definitively observed. Data included in this study were from the other three cats for which an L_0 was definitively observed so that proper scaling and comparisons between the data-sets could be made. For the rest of this paper, an active trial (FL or FV) simply refers to a trial in which the muscle was maximally activated, so that force records include both active AND passive components.

Data were combined from all of the active FL trials for each animal to determine the F_{SE} curve for the connective-tissues. Because of the artifacts encountered in using whole aponeurosis length discussed by Scott and Loeb (1995), only data collected from the distal portion of the aponeurosis were used. All subsequent references to aponeurosis data in this manuscript refer only to the distal portion of the aponeurosis, with the assumption that the proximal portion would produce similar results. The data used in this portion of the study were obtained throughout the rising phase of force production as the muscles were activated from a passive state to a maximally active state.

Data from the passive FL trials were used to determine the F_{PE1} curve. The characterization of the F_{PE2} force was indirect because direct measurements of the F_{PE2} resistive force are not possible. The difference between the recorded force from active FL trials at lengths $<0.75\ L_0$ and a linear extrapolation of force from data between 0.75 and 0.95 L_0 was used as a first approximation of F_{PE2} force (sample shown in Fig. 2B).

The FL curve was determined by using data from active FL trials. To remove the passive component of the total force, the F_{PE1} and F_{PE2} curves were subtracted from the total force recorded in the active FL trials.

The FV curve was determined in several steps. First, both passive forces were subtracted from the total recorded force followed by normalization to the active (isometric) FL curve. As mentioned previously, the lengthening half of the FV relationship measured by Scott and colleagues (1996, Fig. 6) had a residual length

dependency after normalizing to the isometric FL curve. Because the shortening half does not have any residual length dependency, the logical step was to model these two halves independently with separate functions. This had the added effect of keeping the FV relationship continuous but allowing its first derivative to be discontinuous, which is consistent with the separate physiological mechanisms that account for these two domains of the FV relationship. The shortening half of the FV curve was determined by combining the previously normalized data from FV trials at different lengths. The lengthening half of the FV curve was determined by using data from FV trials at only one length ($\sim L_0$) and subsequently adding a length-dependent term to account for the different plateau levels of the FV curve at different lengths.

The procedure for choosing the best fit equations was the same for all of the curves modelled in this paper. Previously used equations from the literature were fit using the Levenberg-Marquardt algorithm (Press *et al.*, 1986; Kaufman *et al.*, 1989), a least-squares non-linear curve-fitting technique. The convergence criteria set for this iterative algorithm was a 0.01% improvement in the numerical error of fit. The data from each cat were fit separately. The errors from the fits were then plotted as a function of the independent variable to determine whether the equations tended to fit poorly over any particular range. If no equation produced an even distribution of error over the entire range, then new equations were developed and tested. To restrict the complexity of the model, candidate functions were arbitrarily limited to three fittable parameters. The total numerical error produced by the fitting algorithm was then compared among those equations producing an even distribution of error, and the function producing the smallest numerical error was identified as the preferred function.

Results

F_{SE} curve

Two equations (2, 3) were tested for the F_{SE} curve. As can be seen in Fig. 3 (a graph of the fits and errors) equation 3 provides a superior fit and so was chosen for the F_{SE} function. Also shown in Fig. 3D, E are graphs of the best fits to the five SE data sets (two tendon data sets and three aponeurosis data sets), using two different scaling parameters for length. In Fig. 3D, length was scaled using the traditional L_s^T as estimated from the original length data, while in Fig. 3E length was scaled using L_0^T. It appears that using L_0^T as the length scaling factor produces more congruent curves.

$$F_{SE}(L^T) = c^T * \{\exp[k^T * (L^T - L_r^T)] - 1\} \quad (2)$$

(Hatze, 1977)

$$F_{SE}(L^T) = c^T * k^T * \ln\left\{\exp\left[\frac{(L^T - L_r^T)}{k^T}\right] + 1\right\} \quad (3)$$

L^T – connective tissue length.

There was a second reason for choosing Equation 3 to model the F_{SE} curve beyond the better fit that it provides. Equation 3 has the form of an exponential at lengths $<L_r^T$, followed by a smooth transition to a straight line at lengths $>L_r^T$. Many researchers have observed that both the F_{PE1} and the F_{SE} have this exact form, but have used two separate equations over the different ranges to model the curves (Otten, 1987; Zajac, 1989). The use of equation 3 removes the need for two separate equations while still retaining the desired shapes over the different ranges. A sample of the curve is shown in Fig. 4 with the effects of each parameter demonstrated; 'c' defines the end-slope of the curve (stiffness), 'k' defines the curvature, and 'L_r' defines the x-axis position (length).

Note that for the SE, use of the normalization constants F_0 and L_0^T defines $F_{SE} = 1$ when $L^T = 1$. Therefore one of the parameters in Equation 3 is redundant. It is trivial to show that for $c^T * k^T < 0.20$, the approximation

$$L_r^T = 1 - \frac{1}{c^T} \quad (4)$$

produces an error in L_r^T of less than 0.04%.

F_{PE1} curve

Two equations of the same form as equations 2 and 3 (replacing L^T with L and the parameters with c_1, k_1 and L_{r1}) were tested for the F_{PE1} curve. As can be seen in Fig. 5 (a graph of the fits and errors) the two equations fit very similarly. Equation 3 had a slightly smaller numerical error and so was chosen as the equation to describe F_{PE1}. As described above, the second reason for choosing equation 3 to model the F_{PE1} curve is because its shape provides a better fit over a wide range with a single equation.

F_{PE2} curve

Unlike the F_{PE1} curve, only one equation (5) was tested for the F_{PE2} curve. The resulting fit and errors are graphed in Fig. 6. All errors were $<0.005\ F_0$ and were equally distributed over the entire range so no other equations were tested.

$$F_{PE2}(L) = c_2 * \{\exp[k_2 * (L - L_{r2})] - 1\} \quad (5)$$

FL curve

Equations 6–9 were fit to the active FL data. The fits and errors produced by these equations are shown in Fig. 7.

$$FL(L) = a * (L - 1)^2 + 1 \quad (6)$$

(Woittiez *et al.*, 1983)

$$FL(L) = \sin(a * L^2 + b * L + c) \quad (7)$$

(He *et al.*, 1991; note: $FL(L = 1.0) = 1.0$ was forced)

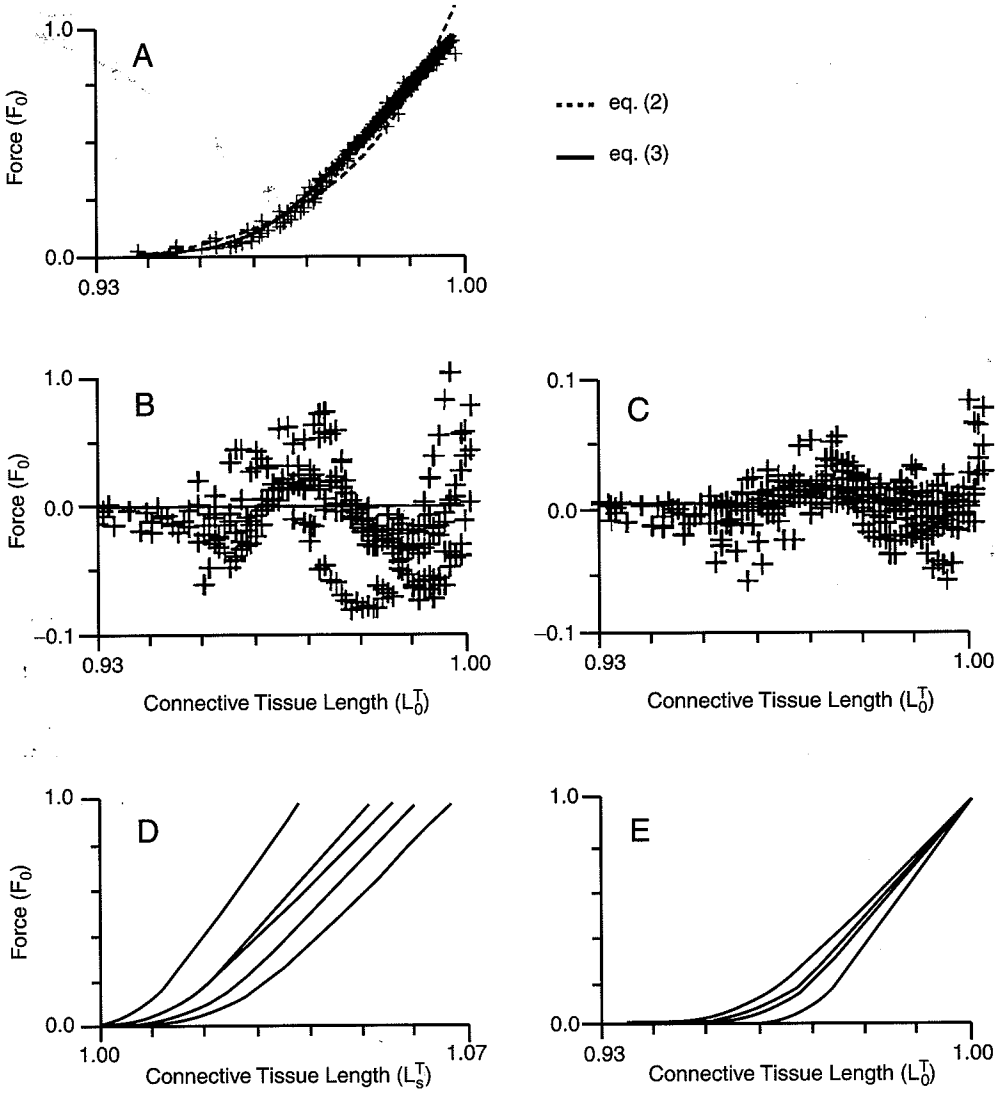

Fig. 3. F_{SE} data, fits and errors. (A) SOL10 aponeurosis data and equations 2 and 3 fit. (B, C) fitting errors (all three cats, including two sets of tendon data and three sets of aponeurosis data, pooled together) from equations 2 and 3 respectively. (D, E) the best fits for the five SE data sets using equation 3 with length scaled by L_s^T and L_0^T respectively.

$$FL(L) = \exp\left\{-\left(\frac{L^\beta - 1}{\omega}\right)^\rho\right\},\ \rho = 2 \qquad (8)$$

(Kaufman *et al.*, 1989)

$$FL(L) = \exp\left\{-\text{abs}\left|\frac{L^\beta - 1}{\omega}\right|^\rho\right\} \qquad (9)$$

(Otten, 1987).

Visually from the error plots in Fig. 7 one can see that equation 9 produced the most accurate fit, and was consistent over the entire range.

FV curve, shortening half

Equations 10 and 11 were fit to the active shortening FV data (with data from all lengths combined as mentioned in Materials and Methods). The fits and errors produced by the equations are shown in Fig. 8.

$$FV_{CON}(V) = \frac{(b_1 - a_1 * V)}{(V + b_1)} \qquad (10)$$

(Hill, 1938, note: V is defined as positive during stretch)

$$FV_{CON}(V) = a_1 * [\exp(b_1 * V) - 1] + 1 \qquad (11)$$

(mathematically equivalent to Aubert, 1956, as cited by Hatze, 1977).

Both equations produced a similar distribution of error (as shown in Fig. 8) and a similar numerical error (with equation 11 perhaps slightly better). However, in all three fits for equation 11 the parameter 'a_1' was calculated to be <1, resulting in an infinite maximum speed of shortening (V_{max}) as

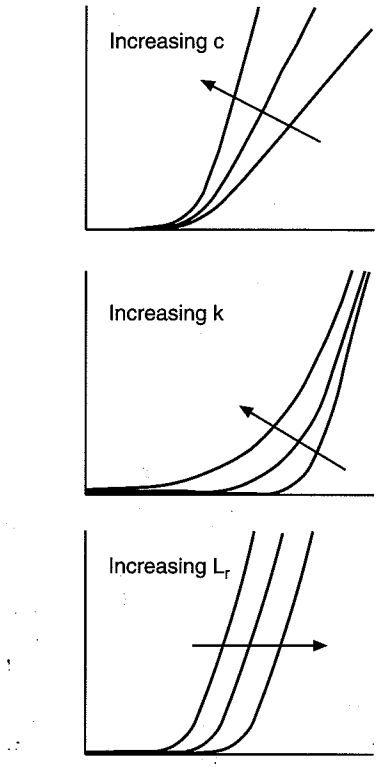

Fig. 4. Effects of individually changing equation 3 parameters. 'c' defines the asymptotic slope (stiffness) of the function, 'k' defines the curvature, and 'L_r' defines the x-axis (length) position.

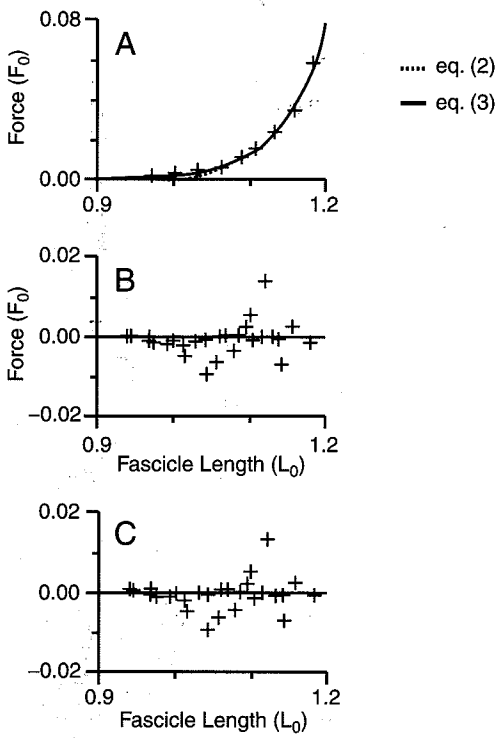

Fig. 5. F_{PE1} data, fits and errors. (A) SOL12 data and equations 2 and 3 fit. (B, C) fitting errors (all three cats pooled together) from equations 2 and 3 respectively.

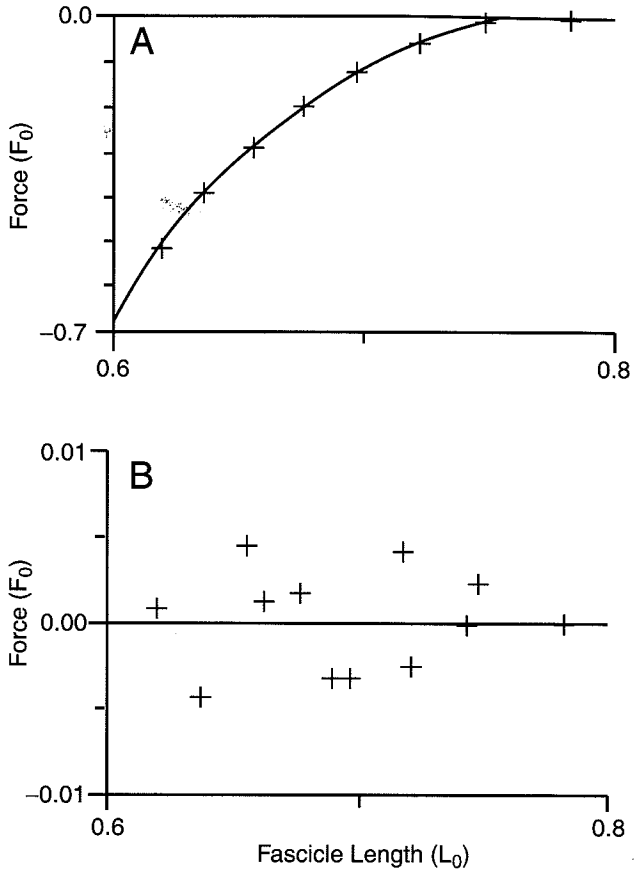

Fig. 6. F_{PE2} data, fits and errors. (A) SOL11 data and equation 5 fit. (B) fitting errors (all three cats pooled together) from equation 5.

suggested in Fig. 8. Studies investigating the shortening of muscles at long lengths (where large passive tension occurs) have shown that muscles can contract at speeds $>V_{max}$ (Seo *et al.*, 1994). The high speeds occur only because of the high passive tension. A calculation of the FV force index from these results, however, produces a negative number. Equation 11 would never be able to model this effect with $a_1 < 1$, and so equation 10 was chosen to describe the shortening half of the FV curve.

FV curve, lengthening half

Equations 12–15 were fit to the active lengthening FV data at one particular length ($\sim L_0$). The fits and errors produced by these equations are shown in Fig. 9.

$$FV_{ECC}(V) = \frac{(b_2 - a_2 * V)}{(V + b_2)} \quad (12)$$

(mathematically equivalent to Mashima *et al.*, 1972)

$$FV_{ECC}(V) = a_2 * [\exp(b_2 * V) - 1] + 1 \quad (13)$$

$$FV_{ECC}(V) = 1 + a_2 * \tanh(b_2 * V) \quad (14)$$

$$FV_{ECC}(V) = 1 + a_2 * \arctan(b_2 * V) \quad (15)$$

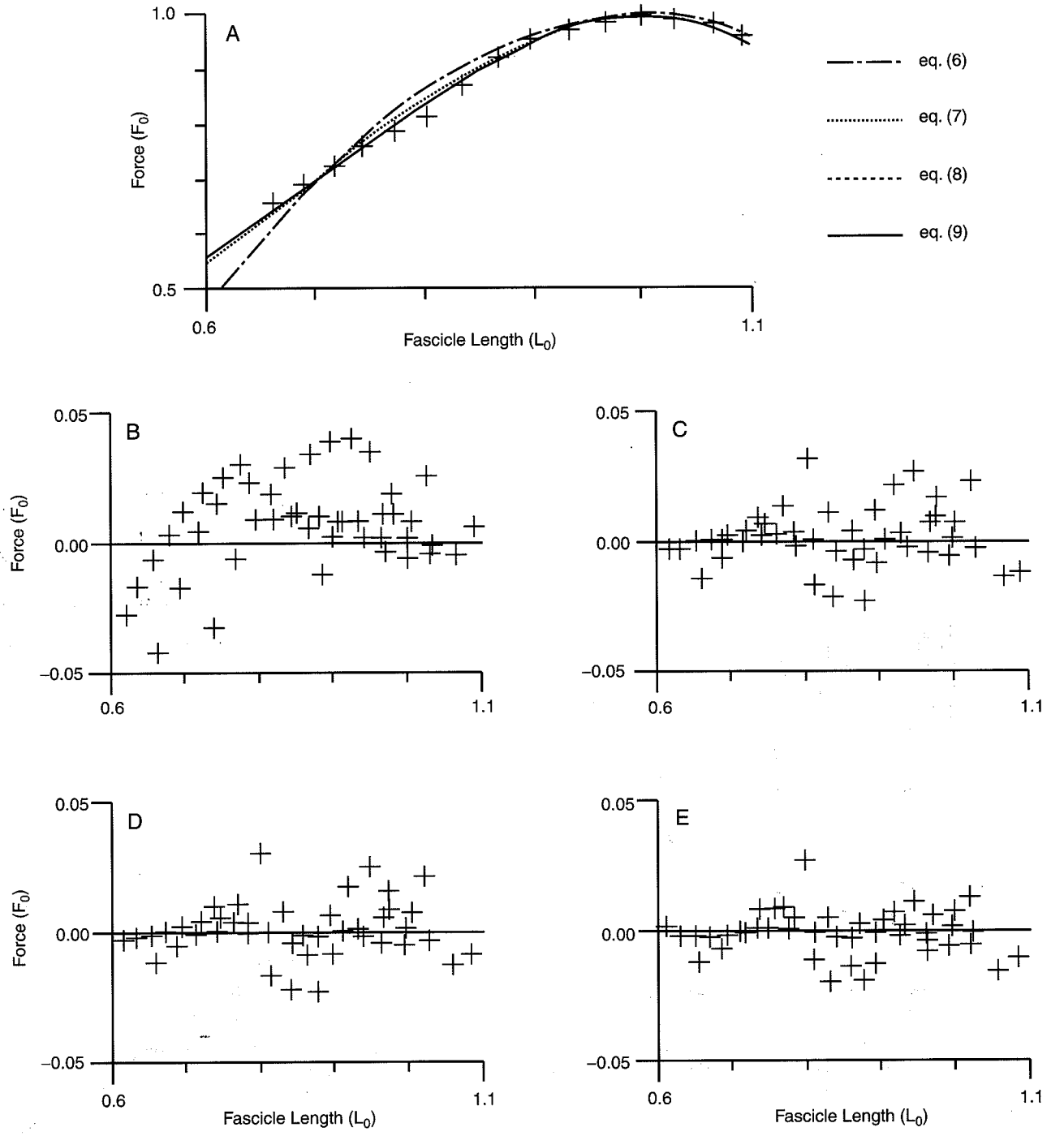

Fig. 7. FL data, fits and errors. (A) SOL12 data and equations 6–9 fit. (B–E) fitting errors (all three cats pooled together) from equations 6–9, respectively.

As can be seen in Fig. 9, all four fits produce slightly different curvatures. An examination of the error distributions suggests that equations 12 and 15 produced the most even distributions of error over the entire range. However, equation 12 consistently produced the least numerical error of all four equations and so was chosen as the best function for the lengthening FV curve.

As mentioned earlier, the lengthening half of the curve had a length dependency associated with it beyond that of the isometric length dependency. The determination of equation 12 as being the best fit for the lengthening half of the FV curve assumed that the choice of best fit equation was not length dependent itself – i.e. the basic curvature remained constant. Examination of equation 12 reveals that the

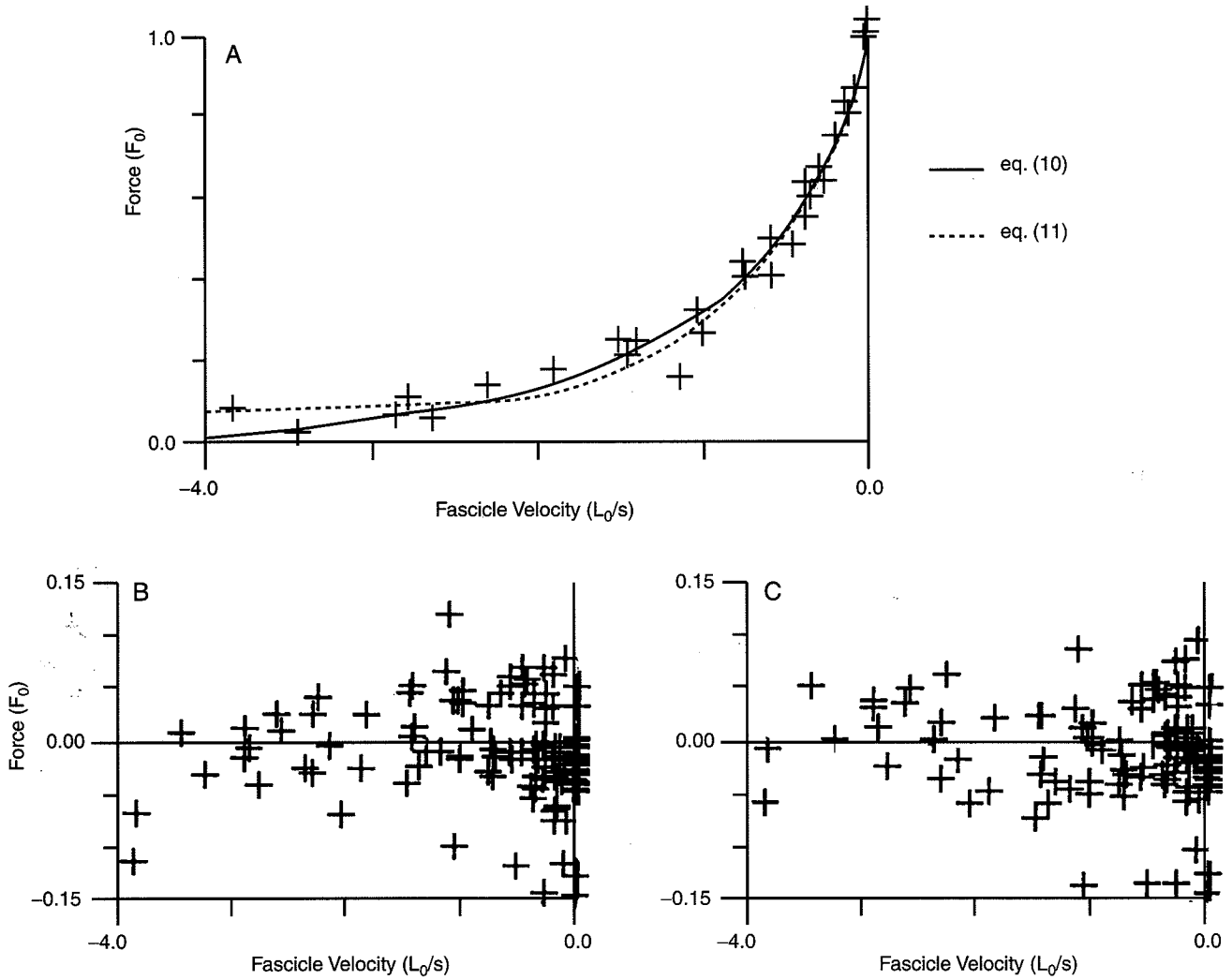

Fig. 8. FV shortening data, fits and errors. (A) SOL12 data and equations 10 and 11 fit. (B, C) fitting errors (all three cats pooled together) from equations 10 and 11 respectively.

maximum force index is determined solely by the constant 'a_2'. To simplify the length dependency of the FV curve, it was assumed that only a_2 was affected by length and not 'b_2'. This assumption is neither supported nor refuted by the data as there were not enough points to test the assumption, rather it was incorporated for simplicity. To determine this extra length dependence, b_2 was first calculated at the length that had the most FV data points. Ideally, this length would have been L_0 for a consistent starting point, but the number of data points available at L_0 was too few to produce a satisfactory fit. Subsequent to the calculation of b_2, a_2 was calculated for each length at which a data set existed using equation 12 with the previously calculated value of b_2. A simple parabola (equation 16) was fit to the a_2 to provide a mathematical description of the length dependence of the FV curve (subsequently called the FI_{max} curve).

$$a_2 = p * L^2 + q * L + r \tag{16}$$

Some comparisons with previous models were made to demonstrate the improvement that could be produced by including a length dependence in the FV curve. Figure 10 compares errors from four equations used previously in the literature (equations 17–20) to those produced by our model. As before, each cat was fit separately and the errors from all cats were plotted on the same graph. A comparison of both the numerical errors (not listed) and the graphs (Fig. 10) demonstrates that the inclusion of length as a variable in the FV curve provides a much improved fit.

$$FV(V) = \begin{cases} \dfrac{(b_1 - a_1 * V)}{(V + b_1)}, & V \leq 0 \\ \dfrac{(b_2 - a_2 * V)}{(V + b_2)}, & V > 0 \end{cases} \tag{17}$$

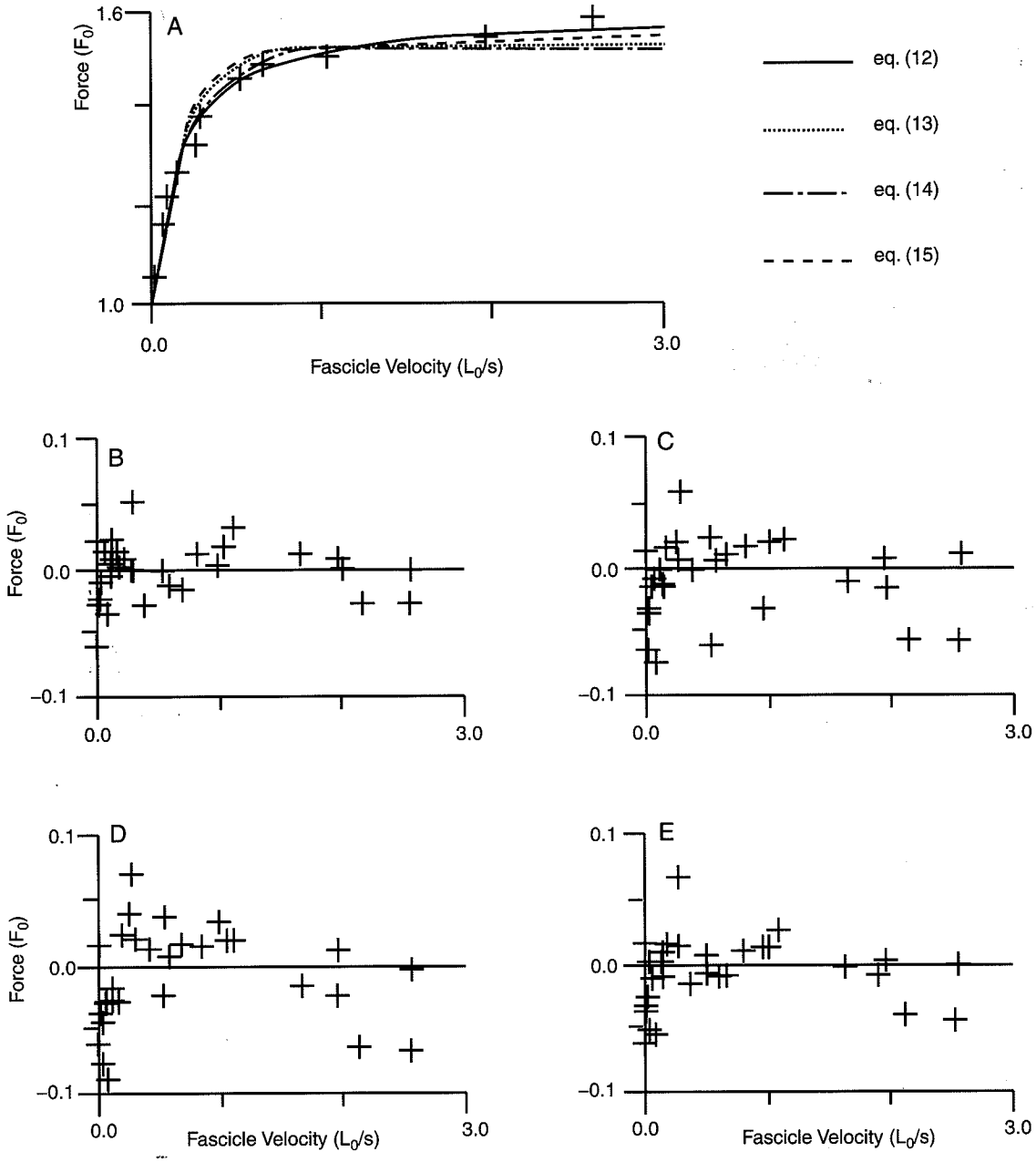

Fig. 9. FV lengthening data, fits and errors. (A) SOL12 data (one trial) and equations 12–15 fit. (B–E) fitting errors (single trials from all three cats pooled together) from equations 12–15 respectively.

(mathematically equivalent to Mashima *et al.*, 1972)

$$FV(V) = a_0*[1 + \tanh[a_1*(V - a_2)]] \quad (18)$$

(Hatze, 1977)

$$FV(V) = \begin{cases} \dfrac{(b_1 - a_1*V)}{(V + b_1)}, & V \le 0 \\ c - z*\dfrac{(c-1)}{(z+V)},\ z = b*\dfrac{(c-1)}{(a+1)} & V \le 0 \end{cases} \quad (19)$$

(Fitzhugh, 1977)

$$FV(V) = 1 + \arctan(a*V^3 + b*V^2 + c*V) \quad (20)$$

(He *et al.*, 1991).

A summary of the best fit parameters for each curve's best fit equation is presented in Table 1. Because the properties of the F_{PE2}, FL, FV and FI_{max} curves are associated with the actin and myosin filaments within sarcomeres, these curves should be consistent among different cats if the data are normalized to properties associated with sarcomeres (L_0 and F_0). Similarly, if one assumes both that the material properties of connective-tissue and the ratio of connective-tissue CSA to muscle PCSA are specimen independent (Zajac, 1989), then F_{SE} curves from different animals also should be congruent if normalized to L_0^T and F_0. Thus the data from all three cats were pooled together to calculate the best fit

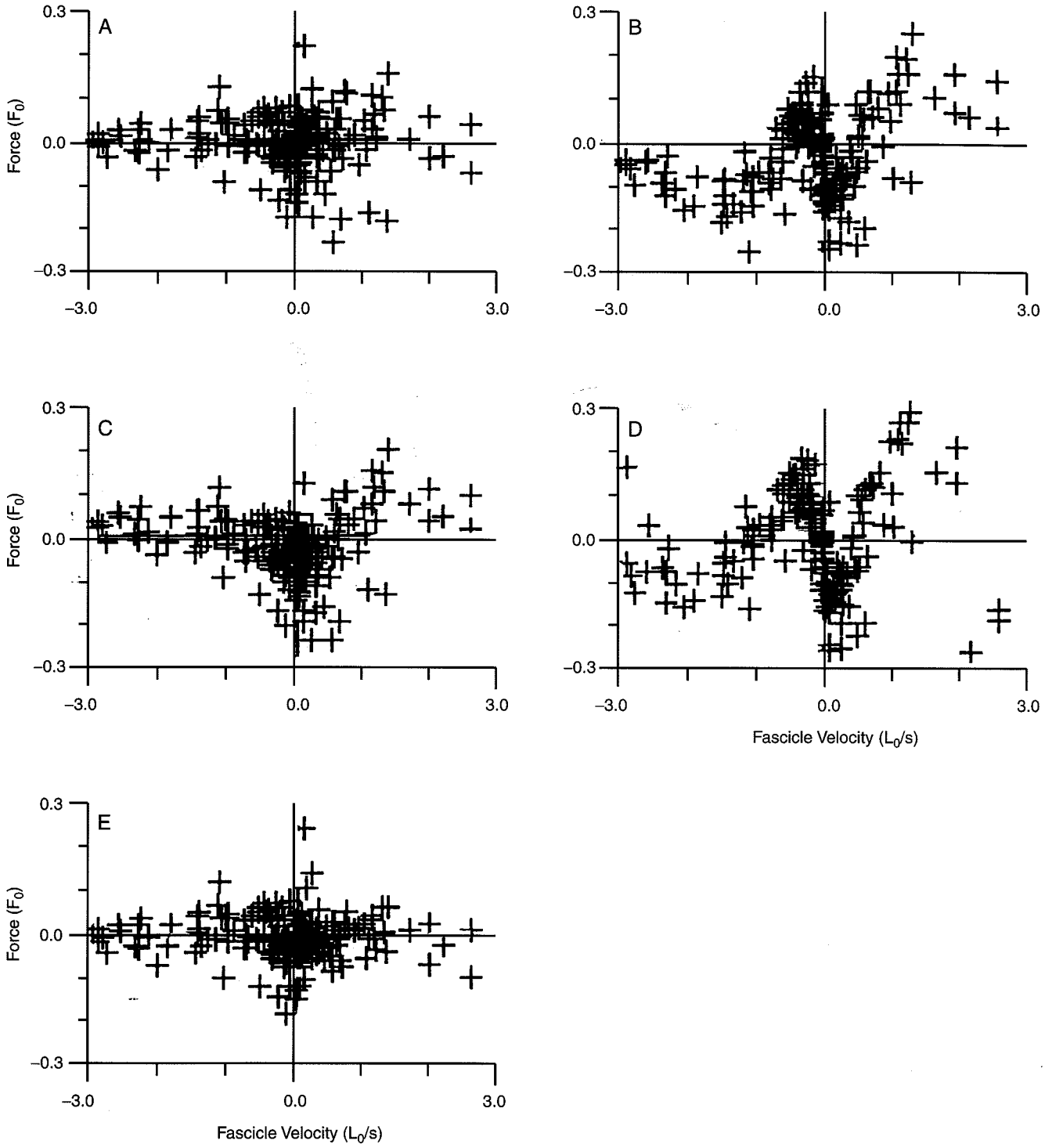

Fig. 10. FV errors. (A–E) fitting errors (all three cats pooled together) from equations 17–20 and 10 and 12 respectively.

parameters for each of these curves. It is not clear, however, whether F_{PE1} would also be expected to normalise between specimens. Magid and colleagues (1984) have shown that in frog semitendinosus muscle, passive tension up to sarcomere lengths of 3.8 μm is due to a third intra-sarcomere myofilament called connectin. Others (Hatze, 1977; Zajac, 1989) suggest that both inter- and intra-fibre factors may play a role, with the contributions from inter- and intra-fibre factors varying between individual muscles. Irrespective of the actual mechanism of passive force, it is independent of actin and myosin overlap, and hence there is no *a priori* reason for passive force to scale between muscles or cats when

Table 1. Best fit constants for best fit equations.

Curve	*Constants*		
F_{SE}–equation 3	c^T	k^T	L_r^{T*}
	27.8	0.0047	0.964
F_{PE1}–equation 3	c_1	k_1	L_{r1}
SOL10	355	0.040	1.35
SOL11	76.4	0.053	1.40
SOL12	67.1	0.056	1.41
F_{PE2}–equation 5	c_2	k_2	L_{r2}
	−0.020	−18.7	0.79
FL–equation 9	ω	β	ρ
	1.26	2.30	1.62
FV–equations 10, 12	a_1	b_1	b_2
	0.17	−0.69	0.18
FI_{max}–equation 16	p	q	r
	−5.34	8.41	−4.70

*As stated earlier, I_r^T is redundant and in this case can be calculated using equation 4; the inclusion of its value in this table was simply for ease of use.

normalized with L_0 and F_0. The data (as presented by Scott *et al.*, 1996, Fig. 4A) used in this study obviously do not scale between cats, which is consistent with previous findings (Woittiez *et al.*, 1983; unpublished personal observations). F_{PE1} was thus fit separately for each cat.

Discussion

The model described here incorporates the salient features, according to objective criteria, from both previously described as well as new model equations. These features are shown graphically in Fig. 11 which contains two three-dimensional plots of muscle force versus fascicle length and velocity based upon the equations and parameters listed in Table 1; the first plot shows active force, whereas the second shows total force (active + passive). Improvements over previous models as well as the limits of this model are discussed below. While many of these improvements are small, they often involve regions of the surface shown in Fig. 11B that are steeply sloped and hence have important implications for motor control.

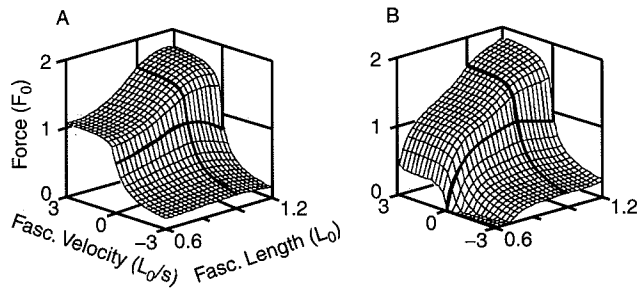

Fig. 11. Three-dimensional views of force produced by the muscle fascicles as a function of length and velocity: (A) active force FLV surface. (B) total (active + passive) force FLV surface.

The model omits two elements that have been included in many previous models: series elasticity within the muscle fascicles (Pierrynowski & Morrison, 1985) and velocity dependence (viscosity) within the PE (Hatze, 1977). The series elasticity within the muscle fascicles is thought to reside within the cross-bridges and perhaps myosin (Pollack, 1983; Pollack & Sugi, 1984) and therefore can act over only a very short range. The velocity-dependent passive force observed in this data set was extremely small, less than 1% of F_0 at the highest velocities (Scott *et al.*, 1996). Both elements would add more complexity than accuracy to a model designed for most physiological conditions, and so neither element was included in this model. However, it may be necessary to include a small viscosity as well as a realistic inertial mass when using any such models to simulate step changes in activation in order to avoid mathematical instability (W. S. Levine, personal communication).

We selected L_0^T as the scaling factor for connective-tissue length rather than the traditional L_s^T. L_s^T can be difficult to measure precisely due to the shape of the F_{SE} curve. Furthermore, Hubbard and Chun (1988) observed that a single stretch of 6% strain can shift L_s^T by 1%, while at higher forces ($\sim F_0$) the shifts were only 0.2%. To demonstrate the problems associated with using L_s^T, we plotted the same five SE curves in Fig. 3D, E, scaled by L_s^T and L_0^T respectively. The variability shown in Fig. 3D compared to Fig. 3E demonstrates the potential for errors when estimating strain using L_s^T. The common past use of L_s^T as a scaling factor could perhaps explain the wide variability of connective-tissue strains reported in the literature for a given stress.

Zajac (1989) explained the rationale for choosing the CE scaling factors L_0 and F_0, which included the critical requirement that the CE be related exclusively to the muscle fascicles. This relationship is intuitively correct because it makes L_0 the length of the anatomical contractile component and F_0 the force produced by the anatomical contractile component (which is proportional to its CSA, assuming negligible pennation angle). Previous models, however, have often related the properties of the CE either to the muscle belly (Woittiez *et al.*, 1983; Kaufman *et al.*, 1989) or to the entire muscle (Fitzhugh, 1977; Baratta *et al.*, 1993; Durfee & Palmer, 1994). The contractile components and scaling factors of these models are therefore related to the anatomical contractile component PLUS connective-tissue, and so Zajac's arguments for choosing L_0 and F_0 as appropriate scaling factors cannot be used. If L_0 and F_0 are used as scaling factors for muscle belly or

whole muscle (as opposed to muscle fascicles), then one should theoretically expect dissimilar results when comparing FL data from different muscles. This problem can be seen clearly in the isometric FL data published by Baratta and colleagues (1993) and Woittiez and colleagues (1983). Woittiez and colleagues (1983) solved this problem (for muscle belly) by introducing an anatomically based index of architecture to account for the change in shape of the FL curve. Unfortunately, their paper did not discuss how the index of architecture could be extended to the FV curve, which seems likely to require more complex dynamic corrections.

A second major problem with the index of architecture is that it assumes an infinitely stiff aponeurosis. Scott and Loeb (1995) observed that the stiffness of aponeurosis is similar to that of tendon. In muscles such as soleus, the aponeurosis is often much longer than the tendon. A model that assumes an infinitely stiff aponeurosis predicts incorrectly the fascicle length and fascicle velocity. This problem is avoided by developing a model that uses anatomically-based components, including an aponeurosis with an accurate stiffness and length.

A limitation in our model's basic design, which is found in all of the models mentioned previously, is the elimination of pennation angle. Zajac (1989) argued that the effects of pennation angle are small enough to be considered negligible for almost all muscles due to their generally small pennation angles and the shape of the sine function that determines this effect. We chose zero pennation angle over varied pennation angle because it is much simpler, and over constant pennation angle because Scott and Winter (1991) showed that assuming a constant pennation angle could produce larger errors than neglecting pennation angle.

The model presented here was designed to capture the salient features of the experiments upon which it was based. As with any model, caution should be exercised in extrapolating it to other muscles and operating conditions. This particular model is limited to the macroscopic response of slow twitch muscle fascicles operating within the ROM of the cat soleus muscle under steady-state conditions of maximal activation. The ROM of some muscles extends to at least 1.5 L_0 (Chanaud *et al.*, 1991; unpublished observations); it remains to be seen if the relationships for soleus (ROM 0.6–1.1 L_0) can be extrapolated to these longer sarcomere lengths. Most muscles are composed of more than one fibre type. Although it has not been tested, we hope that the equations developed here could be applied to more typical muscles with mixed fibre types using different parameters for other fibre types and appropriate weighting coefficients. The practical application of these models to predict force during modulated physiological recruitment awaits the development of models that represent the kinetics of the activation process, which may themselves have length and velocity dependencies.

Acknowledgements

We thank Dr F. J. R. Richmond for helpful comments. This work was supported by the Medical Research Council of Canada.

References

ALLEN, J. D. & MOSS, R. L. (1987) Factors influencing the ascending limb of the sarcomere length-tension relationship in rabbit skinned muscle fibres. *J. Physiol.* **390**, 119–36.

AUBERT, X. (1956) Le couplage energetique de la contraction musculaire. Thesis. Brussels: Arscia.

BARATTA, R., SOLOMONOW, M., BEST, R. & D'AMBROSIA, R. (1993) Isotonic length/force models of nine different skeletal muscles. *Med. Biol. Eng. Comput.* **31**, 449–58.

CHANAUD, C. M., PRATT, C. A. & LOEB, G. E. (1991) Functionally complex muscles of the cat hindlimb. II. Mechanical and architectural heterogeneity in the biceps femoris. *Exp. Brain Res.* **85**, 257–70.

CHIZECK, H. J. (1992) Adaptive and nonlinear control methods for neuroprostheses. In *Neural Prostheses: Replacing Motor Function after Disease or Disability* (edited by STEIN, R. B., PECKHAM, H. P. & POPOVIC, D.) pp. 298–328. New York: Oxford University Press.

DURFEE, W. K. & PALMER, K. I. (1994) Estimation of force-activation, force-length, and force-velocity properties in isolated, electrically stimulated muscle. *IEEE Trans. Biomed. Eng.* **41**, 205–16.

FITZHUGH, R. (1977) A model of optimal voluntary muscular control. *J. Math. Biol.* **4**, 203–36.

GORDON, A. M., HUXLEY, A. F. & JULIAN, F. J. (1966) The variation in isometric tension with sarcomere length in vertebral muscle fibres. *J. Physiol.* **184**, 170–92.

GOSLOW, G. E. J., REINKING, R. M. & STUART, D. G. (1973) The cat step cycle: hindlimb joint angles and muscle lengths during unrestrained locomotion *J. Morphol.* **141**, 1–41.

HATZE, H. (1977) A myocybernetic control model of skeletal muscle. *Biol. Cybern.* **25**, 103–19.

HE, J., LEVINE, W. S. & LOEB, G. E. (1991) Feedback gains for correcting small perturbations to standing pasture. *IEEE Trans. Automatic Control* **36**, 322–32.

HILL, A. V. (1938) The heat of shortening and the dynamic constants of muscle. *Proc. R. Soc. Lond. (Biol.)* **126**, 136–95.

HUBBARD, R. P. & CHUN, K. J. (1988) Mechanical responses of tendons to repeated extension and wait periods. *J. Biomech. Eng.* **110**, 11–19.

HUXLEY, H. E. (1971) The structural basis of muscular contraction. *Proc. R. Soc. Lond. (Biol.)* **178**, 131–49.

JOYCE, G. S., RACK, P. M. H. & WESTBURY, D. R. (1969) Mechanical properties of cat soleus muscle during controlled lengthening and shortening movements. *J. Physiol.* **204**, 461–74.

KAUFMAN, K. R., AN, K. & CHAO, E. Y. S. (1989) Incorporation of muscle architecture into the muscle length-tension relationship. *J. Biomech.* **22**, 943–8.

LIEBER, R. L., BROWN, C. G. & TRESTIK, C. L. (1992) Model of muscle-tendon interaction during frog semitendinosis fixed-end contractions. *J. Biomech.* **25**, 421–8.

LOEB, G. E. (1985) Mononeuron task groups – coping with kinematic heterogeneity. *J. Exp. Biol.* **115**, 137–46.

MAGID, A., TING-BEALL, H. P., CARVELL, M., KONTIS, T. & LUCAVECHE, C. (1984) Connecting filaments, core filaments, and side-struts: a proposal to add three new load-bearing structures to the sliding filament model. In *Contractile Mechanisms in Muscle* (edited by POLLACK, G. H. & SUGI, H.) pp. 307–323. New York: Plenum Publishing Corp.

MASHIMA, H., AKAZAWA, K., KUSHIMA, H. & FUJII, K. (1972) The force-load-velocity relation and the viscous-like force in the frog skeletal muscle. *Jap. J. Physiol.* **22**, 103–20.

OTTEN, E. (1987) A myocybernetic model of the jaw system of the rat. *J. Neurosci. Meth.* **21**, 287–302.

PIERRYNOWSKI, M. R. & MORRISON, J. B. (1985) A physiological model for the evaluation of muscular forces in human locomotion: theoretical aspects. *Math. Biosci.* **75**, 69–101.

POLLACK, G. H. (1983) The cross-bridge theory. *Physiol. Rev.* **63**, 1049–113.

POLLACK, G. H. & SUGI, H, eds (1984) *Contractile Mechanisms in Muscle.* New York: Plenum Publishing Co.

PRESS, W. H., FLANNERY, B. P., TEUKOLSKY, S. A. & VETTERLING, W. T. (1986) *Numerical Recipes.* Cambridge, MA: Cambridge University Press.

SCOTT, S. H. & LOEB, G. E. (1995) The mechanical properties of the aponeurosis and tendon of the cat soleus muscle during whole-muscle isometric contractions. *J. Morphol.* **224**, 73–86.

SCOTT, S. H. & WINTER, D. A. (1991) A comparison of three muscle pennation assumptions and their effect on isometric and isotonic force. *J. Biomech.* **24(2)**, 163–7.

SCOTT, S. H., THOMSON, D. B., RICHMOND, F. J. R. & LOEB, G. E. (1992) Neuromuscular organization of feline anterior sartorius: II. Intramuscular length changes and complex length-tension relationships during stimulation of individual nerve branches. *J. Morphol.* **213**, 171–83.

SCOTT, S. H., BROWN, I. E. & LOEB, G. E. (1996) Mechanics of feline soleus: I. Effect of fascicle length and velocity on force output. *J. Muscle Res. Cell. Motil.* **17**, 207–219.

SEO, J. S., KRAUSE, P. C. & MCMAHON, T. A. (1994) Negative developed tension in rapidly shortening whole frog muscle. *J. Muscle Res. Cell Motil.* **15**, 59–68.

SUGI, H. (1972) Tension changes during and after stretch in frog muscle fibres. *J. Physiol.* **225**, 237–53.

WALMSLEY, B., HODGSON, J. A. & BURKE, R. E. (1978) Forces produced by medial gastrocnemius and soleus muscles during locomotion in freely moving cats. *J. Neurophysiol.* **41**, 1203–16.

WOITTIEZ, R. D., HUIJING, P. A. & ROZENDAL, R. H. (1983) Influence of muscle architecture on the length-force diagram: a model and its verification. *Pflugers Arch.* **397**, 73–4.

ZAJAC, F. E. (1989) Muscle and tendon: properties, models, scaling and application to biomechanics and motor control. *Crit. Rev. Biomed. Eng* **17**, 359–411.